High-density optical interconnects based on self-imaging in coupled waveguide arrays

J. Petrovic*, J. Kršić, A. Maluckov

Vinča Institute of Nuclear Sciences, National Institute of the Republic of Serbia, University of Belgrade, 12-14 Mike Petrovica Alasa, 11000 Belgrade, Serbia

J. J. P. Veerman

Fariborz Maseeh Department of Mathematics and Statistics, Portland State University, Portland, OR, USA

Abstract

Rapidly increasing demand for higher data bandwidths has motivated exploration of new communication channels based on spatially multiplexed in-fibre and on-chip coupled light guides. However, the conventionally used periodically arranged coupled waveguides display complicated light propagation patterns, ranging from quasiperiodic to nearly chaotic. Taking a different approach, we spectrally engineer interwaveguide coupling to instigate self-imaging of the input light state at the array output and thus enable construction of novel high-fidelity interconnects. Simple implementation via modulation of the interwaveguide separations makes these interconnects realizable in all fabrication platforms. Their competitive advantages are a negligible crosstalk-induced information loss, high density that exceeds the current standards by an order of magnitude, and compatibility with both classical and quantum information encoding schemes. Moreover, the wavelength-dependent self-imaging opens up new possibilities for wavelength and spatial division demultiplexing. The proposed analytical designs are supported by extensive numerical simulations of silicon-on-insulator, silicon nitride and silica glass waveguide arrays, and a sta-

*Corresponding author
Email address: jovanap@vin.bg.ac.rs (J. Petrovic)

tistical feasibility study.

Keywords: waveguide arrays, crosstalk, interconnects

1. Introduction

Optical transmission links and interconnect serve the modern industrial and consumer information markets and are seen as platform for future quantum information transfer [1]. Solutions for long-haul data transfer have pushed the signal multiplexing in time and wavelength domains to their technological limits [2, 3, 4]. The Big Data and Internet of Things put additional requirements on the short-range data transfer and routing to and from the network end-points. Finally, fibre-to-chip, intra-chip and on-chip interconnects built into the computer systems and smart phones are facing the input/output (I/O) bottleneck as the packaging density cannot sustain the demand for data bandwidth [5]. Therefore, the innovative solutions for light signal multiplexing and photonic device packaging are in high demand [6, 7].

In the last decade, spatial division multiplexing (SDM) has come to prominence as an underexploited highly-promising resource [8]. Development of optical fibres with multiple single- or multimode cores [9] and multimode waveguides on semiconductor chips [10], opened up new possibilities for mode and path division multiplexing [11]. Albeit compact and effective, the mode division multiplexing is limited by the inter-modal coupling that sets the maximum number of modes or propagation length along the fibre [12]. On the other hand, the first-generation path multiplexing through a bundle of single-core fibres has seen a wide-spread deployment in submarine cables. Due to the increased demand, considerable efforts are being invested in development of the second-generation links based on multicore fibres [13]. However, coupling between closely spaced cores, known as optical crosstalk, limits the link length or the number of cores. Thus the high-throughput transfer can be realized with fibres with large diameters but insufficient mechanical reliability [8]. In the same manner, crosstalk induces losses and limits the packaging density of waveguides in short and on-

chip interconnects [14, 15]. Hence, their usage relies on the crosstalk avoidance and source separation codes [16, 17, 18] or the strategies for waveguide isolation [19, 20, 21, 15], which significantly raises the system complexity and stands in opposition to the low cost per bit requirement. The most successful on-chip crosstalk reduction has been achieved by strong mode confinement in semiconductor interconnects with high refractive index (RI) contrast. Whereas this greatly reduces the footprint with respect to dielectric circuits [22, 23], the fundamental problem of the circuit size being limited by the crosstalk remains.

Consequently, disruptive SDM strategies that leverage on crosstalk have been considered [8]. It was suggested that the signal is encoded in eigenmodes of a coupled system, which propagate undisturbed over large distances [24]. However, complex I/O encoders and decoders are required to project the information to a corresponding eigenbasis. Another solution is provided by multiplexing of the orbital angular momentum (OAM) through multicore fibres with coupled cores [25]. Its prospective deployment depends on the development of sources and couplers for the high-order OAM light. Finally, the recently demonstrated transoceanic distance real-time transmission via a fibre with 4 coupled cores was aided by the time offset between signals in different cores to enable decorrelation at the receiving end [26].

Here, we take a new crosstalk-assisted approach to design high-density waveguide array (WGA) architectures that support high-fidelity on-chip, short-range and long-haul transmission. Our solution leverages on the linear coupling between waveguides to achieve periodic transmission and thus the full restoration of an input state at the output. The periodicity is realized by reverse spectral engineering of WGAs with commensurable eigenfrequencies, hereinafter commensurable waveguide arrays (CWGAs). The purely algebraic commensurability ansatz renders a generic design procedure for a variety of optical interconnects realizable with arbitrary waveguide RI profiles and waveguide densities.

The paper is structured as follows: In Section 1, we explain the idea on a model system composed of discrete nearest-neighbour coupled waveguides. In Section 3, we give examples of interconnects in low, medium and high RI con-

trast materials (silica, silicon nitride and silicon-on-insulator). We numerically estimate the gain in channel density and the classical and quantum link capacity scaling with the number of ports. In Section 4, we discuss the limitations of the model, present results of the feasibility check and estimate permissible fabrication tolerances. We summarize results and give a wider perspective in Section 5.

2. Methods

To demonstrate the commensurability principle and its application in interconnects, we model the waveguide coupling under two simplifying assumptions. The tight-binding approximation (TBA) allows for the representation of the fundamental mode of the j^{th} waveguide by a scalar complex wavefunction $\psi_j(z)$. The nearest-neighbour-coupling approximation yields the following tridiagonal model coupling matrix (Hamiltonian)

$$\mathbf{H} = \begin{pmatrix} \delta_1 & a_{1,2} & \cdots & & \\ a_{2,1} & \delta_2 & & & \\ & & \ddots & & \\ & & & \delta_{M-1} & a_{M-1,M} \\ & & & a_{M,M-1} & \delta_M \end{pmatrix}, \tag{1}$$

where M is the number of waveguides in the array. The coupling matrix is composed of the real coupling coefficients $a_{j,k}$ and the relative phase detunings δ_j of waveguide modes. We assume that all waveguides are identical and hence the modes are phase matched with $\delta_j = 0$, $\forall j$. The propagation of a light state $\psi(z) = (\psi_1(z), \ldots, \psi_i(z), \ldots, \psi_M(z))^T$ along the array is calculated by solving the linear Schrödinger equation and results in

$$\psi(z) = \mathbf{T}\psi(0) = e^{-i\mathbf{H}z}\psi(0), \tag{2}$$

where $\mathbf{T}$ is the transfer matrix. $\mathbf{T}$ describes the functionality of the array and is calculated from the CWGA eigenspectrum by analytic expressions derived in [27].

The state transfer through a WGA interconnect is achieved by selection of the identity transfer matrix, $\mathbf{T}(kL) = \mathbf{I}$, whereby the interconnect length equals k multiples of the revival length L. A trivial analysis of the transfer matrix diagonalised in the form $(\mathbf{D}^{-1}\mathbf{T}\mathbf{D})_{j,k}(z = L) = e^{-i\Lambda_j L}\delta_{j,k}$, where Λ_j are the eigenfrequencies of the coupling matrix $\mathbf{H}$, shows that the equivalence condition is fulfilled for eigenfrequencies $\Lambda_j = n_j 2\pi/L$, where n_j are integers. This is nothing else but the eigenfrequency commensurability condition which ensures that the ratio of any two eigenfrequencies is a rational number.

CWGAs with equal coupling coefficients. In the case of uniform planar arrays, coupling matrix becomes a tridiagonal Toeplitz matrix with the eigenvalues $n_j = 2\cos\frac{m\pi}{M+1}$, $m = 1, 2, \ldots, M$. The arrays with $M < 4$ are periodic. Arrays with $M \geq 4$ have incommensurable eigenspectra and support quasi-periodic light propagation during which the input state is never restored, Fig. 1 f). As a consequence, a uniform WGA is suitable as an SDM interconnect only if the coupling between waveguides can be neglected along the whole array length, which requires large spacing between waveguides and thus limits the interconnect density. Interestingly, the analysis of a circular WGA geometry modelled by a Toeplitz matrix with $a_{M,1} = a_{1,M} \neq 0$, showed that the arrays with $M = 4$ and $M = 6$ waveguides can be stabilized by coupling the first to the end waveguide, while for other values of M also circular systems remain quasiperiodic [28].

CWGAs with unequal coupling coefficients. By allowing for different coupling strengths between the neighbouring waveguides the system coupling matrix becomes a type of Jacobi matrix and acquires new degrees of freedom. The eigenvalues of such a matrix are not readily available analytically [29], which significantly complicates the inverse engineering of CWGA. Particular solutions with Wannier-Stark eigenspectra are found in atoms, molecules or condensed matter systems with spin coupling [30] and their photonic simulators [31, 32]. Due to the unrestricted choice of integers n_j, our model allows for the general solutions beyond the arrays with equidistant eigenfrequencies [33, 34, 31], thus unlocking the potential for design of interconnects and other components, such as couplers and interferometers [35]. Here, we analyse applications of these

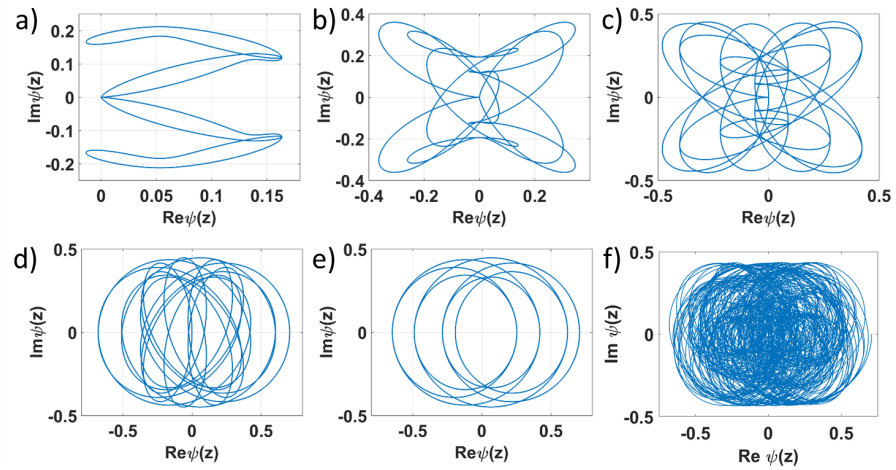

Figure 1: Light propagation through a mirror symmetric CWGA with 9 waveguides and the coupling coefficients $a_{1,2} = a_{8,9} = 1$, $a_{2,3} = a_{7,8} = 3.9965$, $a_{3,4} = a_{6,7} = 6.5000$, $a_{4,5} = a_{5,6} = 6.8516$. Shown are the phase plots of Im$\{\psi(z)\}$ vs. Re$\{\psi(z)\}$ over 100 revival lengths in different waveguides as follows: a) 1 and 9 (end waveguides) b) 2 and 8, c) 3 and 7, d) 4 and 6, and e) 5 (middle waveguide). The input state is $(0, 0, 0, 1, 1, 0, 0, 0, 0)$. f) The corresponding phase plot in waveguide 4 of a WGA with equal coupling coefficients.

solutions in interconnects as SDM systems.

The essential consequence of commensurable spectrum is the highly-ordered periodic light propagation [36, 27]. Its main signatures are the revivals of photon number and relative phases between waveguide modes. The photon number is revived with the maximum fidelity, $F = 1$, defined as $F(z) = (\sum_{j=1}^{M} |\psi_j(z)||\psi_j(0)|)^2$. The analogous result is obtained for the relative phases. Both types of revivals are evidenced in the periodic evolution of the mode wavefunction vectors in the complex plane, Fig. 1 a)-e). In a CWGA, all vectors repeat their paths within each revival length. In a non-commensurable WGA, at least one vector sweeps ever larger part of the complex plane and never repeats its path, Fig. 1 f). Importantly, the revivals are maintained upon any intervention on the input signal, thus allowing for application of different amplitude and phase modulation formats.

The proposed model is ubiquitous and applies to all CWGA embodiments.

Table 1: Properties of waveguides in different materials.

Material	Wavelength [nm]	shape	width [μm]	height [μm]	RI substrate	RI core	RI contrast [%]
SIO	1550	rectangular	0.4	0.3	1.444	3.673	42.3
SiN	800	rectangular	0.5	0.4	1.453	2.020	4.1
SiO_2	800	circular	3.5	3.5	1.453	1.460	0.5
SiO_2 fibre	1550	circular	8.2	8.2	1.445	1.450	0.5

The required coupling coefficients can be delivered by designing interwaveguide separations or RI profiles. The waveguide separations $d_{j,k}$ and coupling coefficients are related by a simple expression $a_{j,k} = Ae^{-\alpha d_{j,k}}$, with the waveguide dependent coupling strength A and decrease rate α, which makes this method simple and fast to implement [37].

3. Results

Based on the transmission length, optical interconnects can be broadly divided into the long-range interconnects with lengths spanning kilometers, short-range interconnects with lengths ranging from meters to centimeters, and on-chip interconnects of centimeter length and shorter. The minimum length of a CWGA interconnect is set by the revival length. Longer interconnects can be trivially realized by using multiple revival lengths. The shorter the revival length, the finer the control of the interconnect length.

Figure 2 compares revival lengths of CWGAs with different RI contrasts given in Table 1 (here defined as $\frac{n_{core}^2 - n_{sub}^2}{2n_{core}^2}$). As there are infinitely many realizations of M-channel CWGA interconnects, all with different coupling coefficients, we find that a waveguide pair ($M = 2$) described by a single coupling coefficient yields the fairest comparison. The revival length for the pair is given by $L = \pi/a$, where the coupling coefficient a exponentially decreases with the waveguide separation. Fine tuning of the waveguide separations allows for the continuous adjustment of the revival length over several orders of magnitude, from 10 μm to over 1 cm in SOI and SiN, from 1 mm to 10 cm on silica chip, and from 1 mm to 1 m in silica fibre.

The revival length further depends on the number of the constituent waveguides M. Here, we circumvent the problem of infinite number of CWGA realizations by providing an estimate for the well-known CWGAs with equidistant eigenfrequencies and spin-inspired coupling coefficients $a_{j,j+1} = \sqrt{j(M-j)}/2$. A simple calculation renders that the period scales as $\sqrt{M}$, which we confirmed numerically. For example, the ratio of the revival length of the interconnect with $M = 13$, Fig. 3 c), and the corresponding 2-waveguide interconnect is $3.5 \approx \sqrt{13/2}$.

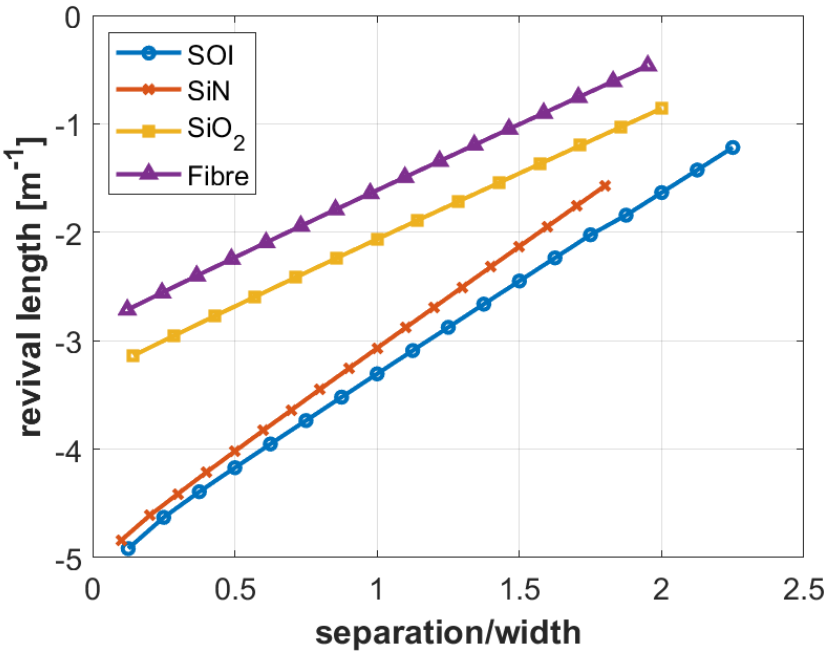

Figure 2: Scaling of the revival length with the interwaveguide separation for a pair of waveguides in different material platforms. A base-10 log scale is used for the Y axis. The waveguide properties are specified in Table 1.

The analytical model of CWGAs works ubiquitously across the fabrication platforms and enables design of interconnects in substrates with different waveguide RI profiles and contrasts. In Fig. 3, we show interconnects on silica-on-insulator (SOI), silicon nitride (SiN) and silicon dioxide (SiO_2) chips, whose

waveguide properties are given in Table 1. For completeness, we also show an interconnect composed of the cores of a typical single-mode step-index fibre. The interconnects in SOI, Fig. 3a), and SiN, Fig. 3b), are composed of rectangular waveguides with the separations by an order of magnitude smaller (few hundreds of nm) than in the conventional crosstalk-avoiding interconnects (few microns) [38]. Their architectures are chosen to demonstrate the flexibility of CWGA design. Namely, both are based on CWGAs that have no other symmetry but the translational along z. Asymmetric CWGAs are fully determined by $M-1$ parameters, whereas the eigenspectrum provides $M/2$ parameters for even M and $(M-1)/2$ for odd M. Additional model parameters that are needed to define an array can be used to optimize the interconnect properties, such as bandwidth or I/O port geometry. On the other hand, the structure of CWGAs with the mirror symmetry is fully defined by their eigenfrequencies, Fig. 3 c), d). As the differences between interwaveguide separations cannot be fully appreciated in the figures, we illustrate them in Fig. 3 d) by propagating a uniform state through a CWGA. The power transfer between waveguides occurs due to the inequality of coupling coefficients.

3.1. Classical link capacity

The capacity C of an SDM communication link can be estimated as $C \sim M \times B$, where M is the number of I/O ports, here simply the number of waveguides, and B is the data transfer rate per I/O port. The data transfer rate depends on multiplexing schemes and the signal-to-noise ratio [1]. In a typical application in which WDM is applied along SDM, B is proportional to the number of wavelength channels.

A particular feature of the WDM in CWGA interconnects is the revival-length dispersion that translates into the dependence of the interconnect length on wavelength. If the dispersion is small enough, all wavelength channels are picked at the same interconnect length and guided further to demultiplexers and demodulators. On the other hand, large dispersion causes differences in interconnect lengths for different wavelength channels and in effect works as a built-in

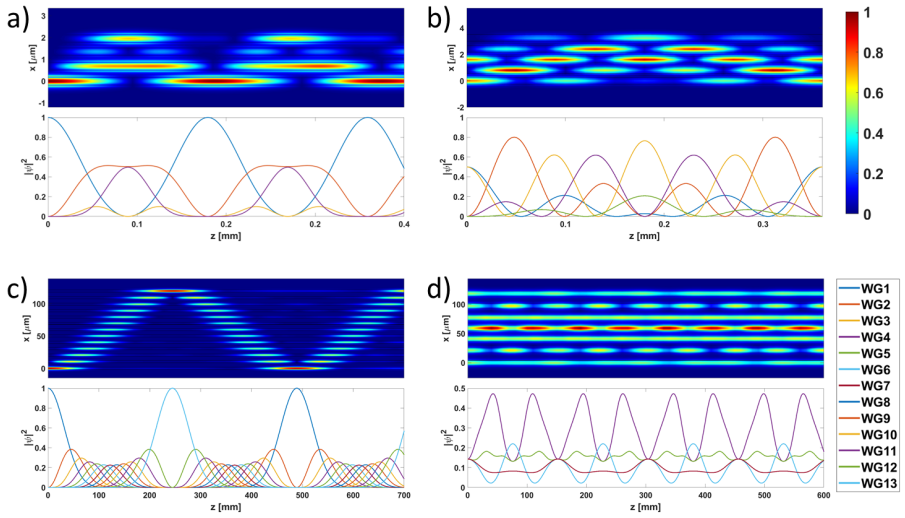

Figure 3: The light propagation through CWGA-based interconnects viewed from above. The light propagates from left to right. a) SOI WGA with 4 waveguides with the minimum separation of 300 nm and coupling coefficients $a_{1,2} = 1$, $a_{2,3} = 1.213$, $a_{3,4} = 2.220$ (color codes WG1-WG4), b) SiN WGA with 5 waveguides at the minimum separation of 300 nm and coupling coefficients $a_{1,2} = 1$, $a_{2,3} = 0.989$, $a_{4,5} = 0.667$,$a_{3,4} = 1.025$ (color codes WG1-WG5), c) SiO_2 WGA with $M = 13$ waveguides at the minimum separation of 7μm and spin-inspired coupling coefficients $a_{j,j+1} = a_{j+1,j} = \sqrt{(M-j)j}/2$ (color codes WG1-WG13), d) An array of 7 SMF-28e optical fibre cores at the minimum separation of 18 μm coupled with the coefficients $a_{1,2} = a_{6,7} = 1$, $a_{2,3} = a_{5,6} = 1.588$, $a_{3,4} = a_{4,5} = 3.111$ (color codes WG1-WG7). The waveguide properties are specified in Table 1.

wavelength demultiplexer, Fig. 4. We have numerically obtained the revival dispersion of an M-channel SDM to be $0.88\sqrt{M/2}$ μm/nm in SOI (waveguides as in Table 1, separated by 300 nm) and $1.68\sqrt{M/2}$ mm/nm in SiO_2 (waveguides as in Table 1, separated by 7 μm). Taking into account the avaliability of ultracompact bend-rejection filters in SOI [39] and glass [40], we infer that the built-in demultiplexer is feasible over the whole C-band for at least 28 SDM channels in SOI and 112 channels in silica. The solution proposed here assumes out-of-plane expansion to accommodate filters. Alternatively, in-plane filters can be implemented at the end of a fanned-out WGA.

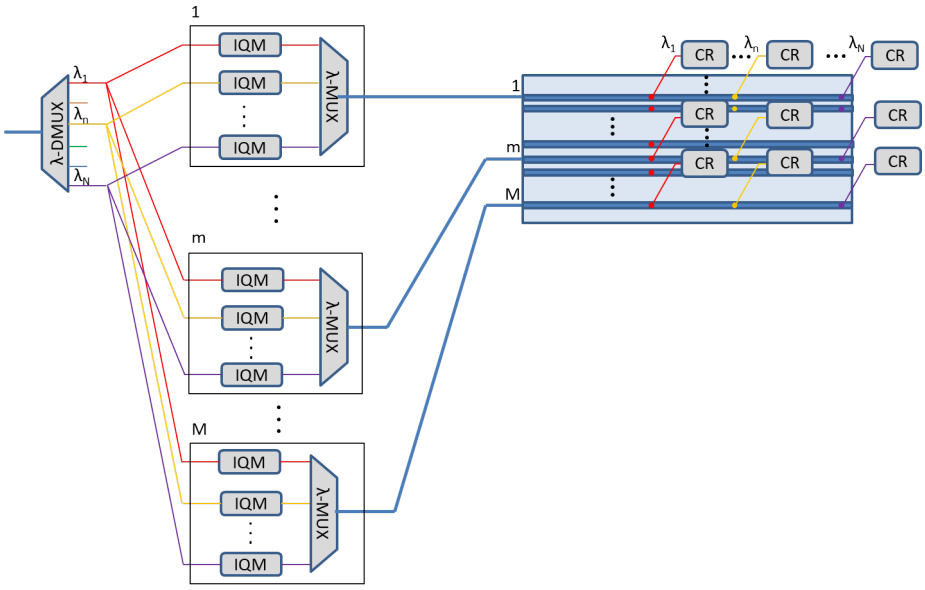

Figure 4: An example WDM-SDM system with a CWGA interconnect with built-in demultiplexer. MUX - multiplexer, IQM - IQ modulator , CR - coherent receiver.

3.2. Quantum link capacity

To assess the suitability of CWGA interconnects for quantum information transfer, we evaluated the revivals of photon-coincidences. Namely, while self-imaging of a single photon corresponds to that of the coherent light, it is the transfer of multiple correlated photons that may yield the quantum advantage. We demonstrate the revivals of photon correlations on a path-entangled photon pair and its separable counterpart. The correlation of the former is represented by a coincidence matrix $\mathbf{\Gamma}^{ent}_{j,k}(z) = |\mathbf{T}_{j,p}(z)\mathbf{T}_{k,p}(z)+e^{-i\phi}\mathbf{T}_{j,q}(z)\mathbf{T}_{k,q}(z)|^2$, and of the latter by $\mathbf{\Gamma}^{sep}_{j,k}(z) = |\mathbf{T}_{j,p}(z)\mathbf{T}_{k,q}(z) + \mathbf{T}_{j,q}(z)\mathbf{T}_{k,p}(z)|^2$, where $\mathbf{T}(z)$ is the CWGA transfer matrix [32]. The revivals are found as occurrences of the perfect overlap of a propagated coincidence matrix with its value at the input to the CWGA, whereby the overlap metric is the matrix similarity $S^{ent/sep} = \frac{\sqrt{(\sum_{j,k}\mathbf{\Gamma}^{ent/sep}_{j,k}(z=0)\mathbf{\Gamma}^{ent/sep}_{j,k}(z))^2}}{\sum_{j,k}\mathbf{\Gamma}^{ent/sep}_{j,k}(0)\sum_{j,k}\mathbf{\Gamma}^{ent/sep}_{j,k}(z)}$ [41]. Results show that both coincidence matrices experience periodic revivals, hence that the path entanglement is fully transferred, Fig. 5.

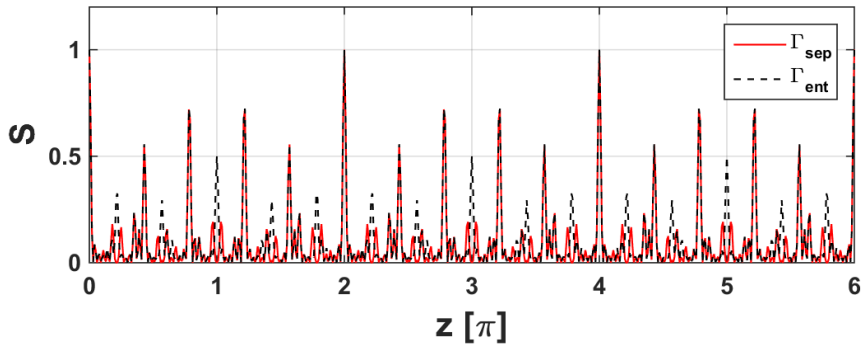

Figure 5: Similarity of the coincidence matrices of a separable (solid line) and correlated (dashed line) photon pairs inserted into waveguides 4 and 5 of the CWGA from Fig. 1. For the generality of the model, the revival length is normalized to 2π.

Quantum states can be encoded into different light properties, notably by the single-rail encoding into photon number and by d-rail encoding into different modes of the system (polarization, orbital angular momentum or waveguide modes) [42, 43, 44]. CWGA interconnects support all these encodings. Specifically, absence of bend-induced losses makes an M-waveguide CWGA suitable for transfer of M single-rail qubits encoded into M photons. The same array can carry $M/2$ dual-rail encoded qubits, each encoded into a single photon and 2 waveguides, or M/d d-iary qudits, each encoded into a single photon distributed over d waveguides. Alternatively, in the spirit of Cerf-Adami-Kwiat protocol [45], an M-waveguide CWGA can transmit $\log_2 M$ qubits or $\log_d M$ d-iary qudits encoded in a single photon distributed over the entire array.

4. Discussion

The main benefits of the crosstalk-friendly interconnects with respect to the conventional ones are the elimination of the crosstalk-induced information loss and increase in interconnect density. We have numerically demonstrated an order of magnitude reduction in the channel separation while maintaining the maximum transfer fidelity. The simulations were within the limits of validity of

the nearest-neighbour coupling assumed in our model. However, the commensurability principle can be applied also to the arrays with significant long-range coupling by adding further side diagonals to the coupling matrix. In the asymptotic case of zero interwaveguide separation, array waveguides merge into a large bulk multimode waveguide and lose the advantage of singlemodedness. This advantage is important as it can provide automatic mode matching with the in- and out-coupling waveguides. Hence, the minimum interwaveguide separations are limited from below by the efficiency of light coupling into and out of CWGA. In the conventional circuits, such as multimode interference multiports, this is resolved by fanning the waveguides out, whereby the footprint of the coupling region dominates the interconnect. On the other hand, huge efforts put in investigation of WGA-based circuit components[35, 46, 47], along with the existing classical and quantum on-chip sources[48, 49] and detectors [50, 51], indicate the possibility of achieving all-WGA bend-free photonic integrated circuits. Having the fabrication technology in place, a challenge before their realization are the demanding procedures for design of WGA-based components. The commensurability approach presented here is a steppingstone to this vision.

Finally, we report results of a comprehensive statistical feasibility check of CWGA fabrication. Dependence of the coupling coefficients and mode detunings (propagation constants) on the waveguide separations and RI profiles makes CWGA susceptible to the fabrication errors. The fabrication errors introduce quenched (z-invariant) and non-quenched (random changes along z) disorder to the system. Simulations have shown that these disorders lead to the same deterioration of fidelity, hence we concentrated on the non-quenched disorder. We first used an implementation-nonspecific model of disorder in the coupling coefficients and detunings, which introduces the normal distribution of variations around their design values with the relative standard deviations σ_{coupl} and σ_{det}, respectively. To link this to a CWGA implementation of interest, we translated these relative standard deviations to those of the waveguide RI contrast and separations, respectively. Since the mean fidelity converged to dramatically different values for different input states and CWGA architectures, we ensured the

'worst-case' scenario by calculating the minimum mean fidelity across all input states.

Results in Fig. 6 show that the variation in coupling coefficients consistently reduces the transfer fidelity by two orders of magnitude faster than the variation in detunings. In particular, to reach fidelity $F > 0.95$, the coupling-coefficient tolerance should not exceed 0.35%, while the margin for detuning remains above 10%. The dominance of the coupling disorder, further amplified by the exponential dependence of the coupling coefficient on the waveguide separation, unambiguously defines the waveguide separation as the critical fabrication parameter. For example, an optimised SiN CWGA interconnect may tolerate 20 nm error in waveguide separations and 0.2 error in the core RI. Experimental demonstrations of the spin-simulating CWGAs show that the proposed interconnects can be accessed by the existing fabrication techniques, such as direct laser writing in glass [31, 37, 32] and lithography and reactive ion etching of semiconductors [41].

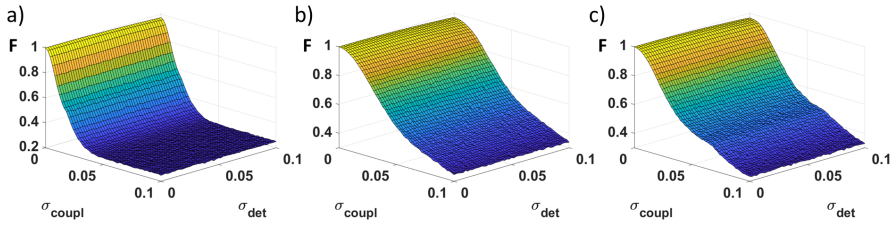

Figure 6: Fidelity in the presence of disorder in the coupling coefficients with the relative standard deviation σ_{coupl} and detunings with the relative standard deviation σ_{det}. Shown is the minimum fidelity across all possible initial states for the first revival in 5-waveguide CWGA interconnects with the coupling coefficients $a_{1,2} = a_{4,5} = 1$ and a) $a_{2,3} = a_{3,4} = 1.543$, b) $a_{2,3} = a_{3,4} = 0.624$ and c) $a_{2,3} = a_{3,4} = 2.739$.

5. Conclusion

We have addressed the challenge of constructing high density SDM links with interchannel crosstalk. The solution is based on CWGAs which support the full

revival of any input state at the output. It is implemented by deriving the CWGA coupling matrix from a chosen commensurable eigenspectrum and adjusting the interwaveguide separations to attain the design coupling coefficients. The proposed approach enables construction of high-density interconnects with negligible crosstalk-induced losses and the length tuneable over several orders of magnitude. They are accessible to the existing fabrication methods. Numerical simulations have shown a 10-fold increase in channel density. Relaxation of the tight-binding and nearest-neighbour approximations enables further increase up to the limits set by the specific output coupler size and efficiency. Even greater gains in footprint are expected in multiport WGA components without a preset length, such as couplers and interferometers. We see the proposed interconnects as a component of the future photonic integrated circuits composed solely of WGAs. The findings of this paper and the recent works of others show that such circuits are capable of handling both classical and quantum information, thus paving the way to the realization of ultimately small energy-efficient optical communication, computation and sensing hardware.

Acknowledgement

J. P., J.K. and A. M. acknowledge support from the Ministry of Education, Science, and Technological Development of the Republic of Serbia, Grant No. 451-03-68/2020-14/200017. J. P. acknowledges useful discussions with U. Woggon and A. Achstein and M. Kleinert's generous help with defining SiN waveguide properties.

References

[1] W. Shi, Y. Tian, A. Gervais, Scaling capacity of fiber-optic transmission systems via silicon photonics, Nanophotonics 9 (16) (2020) 4629–4663. doi:doi:10.1515/nanoph-2020-0309.
URL https://doi.org/10.1515/nanoph-2020-0309

[2] G. Bosco, V. Curri, A. Carena, P. Poggiolini, F. Forghieri, On the performance of nyquist-wdm terabit superchannels based on pm-bpsk, pm-qpsk, pm-8qam or pm-16qam subcarriers, Journal of Lightwave Technology 29 (1) (2011) 53–61. doi:10.1109/JLT.2010.2091254.

[3] A. Arnould, A. Ghazisaeidi, D. Le Gac, P. Brindel, M. Makhsiyan, K. Mekhazni, F. Blache, N. Fontaine, D. Neilson, R. Ryf, H. Chen, M. Achouche, J. Renaudier, 103 nm ultra-wideband hybrid raman/soa transmission over 3 × 100 km ssmf, Journal of Lightwave Technology 38 (2) (2020) 504–508. doi:10.1109/JLT.2019.2946590.

[4] M. Ionescu, D. Lavery, A. Edwards, E. Sillekens, D. Semrau, L. Galdino, R. I. Killey, W. Pelouch, S. Barnes, P. Bayvel, 74.38 tb/s transmission over 6300 km single mode fibre enabled by c+l amplification and geometrically shaped pdm-64qam, Journal of Lightwave Technology 38 (2) (2020) 531–537. doi:10.1109/JLT.2019.2954458.

[5] L. Alloatti, High-speed photonics for side-by-side integration with billion transistor circuits in unmodified cmos processes, Journal of Lightwave Technology 35 (6) (2017) 1168–1173. doi:10.1109/JLT.2017.2655420.

[6] J. Zhang, Z. Jia, Coherent passive optical networks for 100g/λ;-and-beyond fiber access: Recent progress and outlook, IEEE Network 36 (2) (2022) 116–123. doi:10.1109/MNET.005.2100604.

[7] D. A. B. Miller, Device requirements for optical interconnects to silicon chips, Proceedings of the IEEE 97 (7) (2009) 1166–1185. doi:10.1109/JPROC.2009.2014298.

[8] B. J. Puttnam, G. Rademacher, R. S. Luís, Space-division multiplexing for optical fiber communications, Optica 8 (9) (2021) 1186–1203. doi:10.1364/OPTICA.427631.
URL http://opg.optica.org/optica/abstract.cfm?URI=optica-8-9-1186

[9] Y. Yadin, M. Orenstein, Parallel optical interconnects over multimode waveguides using mutually coherent channels and direct detection, J. Lightwave Technol. 25 (10) (2007) 3126–3131.
URL http://opg.optica.org/jlt/abstract.cfm?URI=jlt-25-10-3126

[10] H. Xu, D. Dai, Y. Shi, Silicon integrated nanophotonic devices for on-chip multi-mode interconnects, Applied Sciences 10 (18). doi:10.3390/app10186365.
URL https://www.mdpi.com/2076-3417/10/18/6365

[11] S. Murshid, B. Grossman, P. Narakorn, Spatial domain multiplexing: A new dimension in fiber optic multiplexing, Optics and Laser Technology 40 (8) (2008) 1030–1036. doi:https://doi.org/10.1016/j.optlastec.2008.03.001.
URL https://www.sciencedirect.com/science/article/pii/S003039920800042X

[12] S. Savović, A. Djordjevich, A. Simović, B. Drljača, Influence of mode coupling on three, four and five spatially multiplexed channels in multimode step-index plastic optical fibers, Optics and Laser Technology 106 (2018) 18–21. doi:https://doi.org/10.1016/j.optlastec.2018.03.015.
URL https://www.sciencedirect.com/science/article/pii/S0030399218302044

[13] C. Papapavlou, K. Paximadis, D. Uzunidis, I. Tomkos, Toward sdm-based submarine optical networks: A review of their evolution and upcoming trends, Telecom 3 (2) (2022) 234–280.

[14] M. Haurylau, et al., On-chip optical interconnect roadmap: Challenges and critical directions, IEEE Journal of Selected Topics in Quantum Electronics 12 (6) (2006) 1699–1705.
URL https://doi.org/10.1109/JSTQE.2006.880615

[15] W. Song, et al., High-density waveguide superlattices with low crosstalk,

Nature Communications 6 (1) (2015) 2027.
URL https://doi.org/10.1038/ncomms8027

[16] C. Qiao, R. Melhem, D. Chiarulli, S. Levitan, A time domain approach for avoiding crosstalk in optical blocking multistage interconnection networks, Journal of Lightwave Technology 12 (10) (1994) 1854–1862. doi:10.1109/50.337500.

[17] Y. Xiong, Y. Ye, H. Zhang, J. He, B. Wang, K. Yang, Deep learning and hierarchical graph-assisted crosstalk-aware fragmentation avoidance strategy in space division multiplexing elastic optical networks, Optics Express 28 (3) (2020) 2758–2777.
URL https://doi.org/10.1364/OE.381551

[18] C. Huang, D. Wang, W. Zhang, B. Wang, A. N. Tait, T. F. de Lima, B. J. Shastri, P. R. Prucnal, High-capacity space-division multiplexing communications with silicon photonic blind source separation, J. Lightwave Technol. 40 (6) (2022) 1617–1632.
URL http://opg.optica.org/jlt/abstract.cfm?URI=jlt-40-6-1617

[19] Y. Yang, Y. Guo, Y. e. a. Huang, Crosstalk reduction of integrated optical waveguides with nonuniform subwavelength silicon strips, Scientific Reports 10 (2020) 4491.
URL https://doi.org/10.1038/s41598-020-61149-1

[20] Y. Bian, Q. Ren, L. Kang, Y. Qin, P. L. Werner, D. H. Werner, Efficient cross-talk reduction of nanophotonic circuits enabled by fabrication friendly periodic silicon strip arrays, Scientific reports 7 (1) (2017) 1–9.
URL https://doi.org/10.1038/s41598-017-16096-9

[21] D. Kwong, et al., Corrugated waveguide-based optical phased array with crosstalk suppression, IEEE Photonics Technology Letters 26 (10) (2014) 991–994.
URL https://doi.org/10.1109/LPT.2014.2311454

[22] Y. Urino, et al., First demonstration of high density optical interconnects integrated with lasers, optical modulators, and photodetectors on single silicon substrate, Optics Express 19 (26) (2011) B159–B165.
URL https://doi.org/10.1364/OE.19.00B159

[23] M. Smit, et al., An introduction to inp-based generic integration technology, Semiconductor Science and Technology 29 (8) (2014) 083001.
URL https://doi.org/10.1088/0268-1242/29/8/083001

[24] Y. Okawachi, O. Kuzucu, M. A. Foster, R. Salem, A. C. Turner-Foster, A. Biberman, N. Ophir, K. Bergman, M. Lipson, A. L. Gaeta, Characterization of nonlinear optical crosstalk in silicon nanowaveguides, IEEE Photonics Technology Letters 24 (3) (2011) 185–187.
URL https://doi.org/10.1109/LPT.2011.2177080

[25] L. Hadžievski, A. Maluckov, A. M. Rubenchik, S. Turitsyn, Stable optical vortices in nonlinear multicore fibers, Light: Science & Applications 4 (8) (2015) e314. doi:10.1038/lsa.2015.87.

[26] S. Beppu, M. Kikuta, K. Igarashi, H. Mukai, M. Shigihara, Y. Saito, D. Soma, H. Takahashi, N. Yoshikane, I. Morita, M. Suzuki, T. Tsuritani, Real-time transoceanic coupled 4-core fiber transmission, in: Optical Fiber Communication Conference (OFC) 2021, Optica Publishing Group, 2021, p. F3B.4. doi:10.1364/OFC.2021.F3B.4.
URL http://opg.optica.org/abstract.cfm?URI=OFC-2021-F3B.4

[27] J. Petrovic, J. Veerman, A new method for multi-bit and qudit transfer based on commensurate waveguide arrays, Annals of Physics 392 (2018) 128–141.
URL https://doi.org/10.1016/j.aop.2018.03.008

[28] A. Radosavljević, et al., Coherent light propagation through multicore optical fibers with linearly coupled cores, Journal of Optical Society of America B 32 (12) (2015) 2520–2527.
URL https://doi.org/10.1364/JOSAB.32.002520

[29] G. Meurant, A review on the inverse of symmetric tridiagonal and block tridiagonal matrices, SIAM Journal on Matrix Analysis and Applications 13 (3) (1992) 707–728. doi:10.1137/0613045.
URL https://doi.org/10.1137/0613045

[30] J. Petrovic, et al., A multi-state interferometer on an atom chip, New Journal of Physics 15 (4) (2013) 043002.
URL https://doi.org/10.1088/1367-2630/15/4/043002

[31] M. Bellec, G. M. Nikolopoulos, S. Tzortzakis, Faithful communication hamiltonian in photonic lattices, Optics Letters 37 (21) (2012) 4504–4506.
URL https://doi.org/10.1364/OL.37.004504

[32] M. Gräfe, A. Szameit, Integrated photonic quantum walks, Journal of Physics B: Atomic, Molecular and Optical Physics 53 (7) (2020) 073001. doi:10.1088/1361-6455/ab6cfc.
URL https://doi.org/10.1088%2F1361-6455%2Fab6cfc

[33] R. J. Chapman, et al., Experimental perfect state transfer of an entangled photonic qubit, Nature Communications 7 (2016) 11339.
URL https://doi.org/10.1038/ncomms11339

[34] R. Gordon, Harmonic oscillation in a spatially finite array waveguide, Opt. Lett. 29 (23) (2004) 2752–2754. doi:10.1364/OL.29.002752.
URL http://opg.optica.org/ol/abstract.cfm?URI=ol-29-23-2752

[35] J. Petrovic, Multiport waveguide couplers with periodic energy exchange, Optics letters 40 (2) (2015) 139–142.
URL ttps://doi.org/10.1364/OL.40.000139

[36] N. K. Efremidis, D. N. Christodoulides, Revivals in engineered waveguide arrays, Optics communications 246 (4-6) (2005) 345–356.
URL https://doi.org/10.1016/j.optcom.2004.11.009

[37] A. Szameit, S. Nolte, Discrete optics in femtosecond-laser-written photonic structures, Journal of Physics B: Atomic, Molecular and Optical Physics

43 (16) (2010) 163001.
URL https://doi.org/10.1088/0953-4075/43/16/163001

[38] V. Donzella, S. T. Fard, L. Chrostowski, Study of waveguide crosstalk in silicon photonics integrated circuits, in: P. Cheben, J. Schmid, C. Boudoux, L. R. Chen, A. Delâge, S. Janz, R. Kashyap, D. J. Lockwood, H.-P. Loock, Z. Mi (Eds.), Photonics North 2013, Vol. 8915, International Society for Optics and Photonics, SPIE, 2013, pp. 291 – 298. doi:10.1117/12.2042366.
URL https://doi.org/10.1117/12.2042366

[39] A. Morand, Y. Zhang, B. Martin, K. P. Huy, D. Amans, P. Benech, J. Verbert, E. Hadji, J.-M. Fédéli, Ultra-compact microdisk resonator filters on soi substrate, Opt. Express 14 (26) (2006) 12814–12821. doi:10.1364/OE.14.012814.
URL http://opg.optica.org/oe/abstract.cfm?URI=oe-14-26-12814

[40] G. Zhang, G. Cheng, M. K. Bhuyan, C. D'Amico, Y. Wang, R. Stoian, Ultrashort bessel beam photoinscription of bragg grating waveguides and their application as temperature sensors, Photon. Res. 7 (7) (2019) 806–814. doi:10.1364/PRJ.7.000806.
URL http://opg.optica.org/prj/abstract.cfm?URI=prj-7-7-806

[41] A. Peruzzo, et al., Quantum walks of correlated photons, Science 329 (5998) (2010) 1500–1503. doi:10.1126/science.1193515.
URL https://science.sciencemag.org/content/329/5998/1500

[42] Y. Wang, Z. Hu, B. C. Sanders, S. Kais, Qudits and high-dimensional quantum computing, Frontiers in Physics 8 (2020) 479. doi:10.3389/fphy.2020.589504.
URL https://www.frontiersin.org/article/10.3389/fphy.2020.589504

[43] D. Drahi, et al., Entangled resource for interfacing single- and dual-rail optical qubits, Quantum 5 (2021) 416. doi:10.22331/q-2021-03-23-416.
URL https://doi.org/10.22331/q-2021-03-23-416

[44] D. K. Burgarth, V. Giovannetti, Dual- and Multi-rail Encoding, Springer Berlin Heidelberg, Berlin, Heidelberg, 2014, pp. 87–122. doi:10.1007/978-3-642-39937-4_3.
URL https://doi.org/10.1007/978-3-642-39937-4_3

[45] N. J. Cerf, C. Adami, P. G. Kwiat, Optical simulation of quantum logic, Phys. Rev. A 57 (1998) R1477–R1480. doi:10.1103/PhysRevA.57.R1477.
URL https://link.aps.org/doi/10.1103/PhysRevA.57.R1477

[46] Y. Franz, M. Guasoni, Compact 1 × n power splitters with arbitrary power ratio for integrated multimode photonics, Journal of Optics 23 (9) (2021) 095802. doi:10.1088/2040-8986/ac1830.
URL https://doi.org/10.1088/2040-8986/ac1830

[47] Y. Lahini, G. R. Steinbrecher, A. D. Bookatz, D. Englund, Quantum logic using correlated one-dimensional quantum walks, npj Quantum Inf 4 (2018) 2. doi:10.1038/s41534-017-0050-2.
URL https://doi.org/10.1038/s41534-017-0050-2

[48] Z. Zhou, B. Yin, J. Michel, On-chip light sources for silicon photonics, Light: Science & Applications 4 (11) (2015) e358.

[49] P. Senellart, G. Solomon, A. White, High-performance semiconductor quantum-dot single-photon sources, Nature nanotechnology 12 (11) (2017) 1026–1039.

[50] W. Yang, J. Chen, Y. Zhang, Y. Zhang, J.-H. He, X. Fang, Silicon-compatible photodetectors: trends to monolithically integrate photosensors with chip technology, Advanced Functional Materials 29 (18) (2019) 1808182.
URL https://doi.org/10.1002/adfm.201808182

[51] W. H. Pernice, C. Schuck, O. Minaeva, M. Li, G. Goltsman, A. Sergienko, H. Tang, High-speed and high-efficiency travelling wave single-photon de-

tectors embedded in nanophotonic circuits, Nature communications 3 (1) (2012) 1–10.